Front. Chem. Sci. Eng. 2025, 19(7): 58
https://doi.org/10.1007/s11705-025-2563-0

RESEARCH ARTICLE

Carbon dioxide conversion and characterization of microwave-induced plasma

Balázs Péter Kiss[1,2], Csenge Emese Toth[1], István Slezsak[2], Zsolt Dobo (✉)[1], George Kaptay[1,3]

1 University of Miskolc, Egyetemvaros, Miskolc 3515, Hungary
2 Innovation Laboratory Ltd., Budapest 1042, Hungary
3 HUN-REN-ME on Materials Sicence, Miskolc 3515, Hungary

Abstract Microwave-induced non-thermal plasma technology is a promising solution to dissociate carbon dioxide, opening the possibility of carbon dioxide upgrade to value-added products and therefore providing an attractive approach in recent decarbonization endeavors. This study aims to comprehensively characterize and optimize microwave-induced pure carbon dioxide plasma focusing on the enhancement of conversion and energy efficiency. Analysis of optical emission spectra and gas composition under varying flow rates, introduced microwave power, and operating pressures was performed, while specific calculations were applied to support the measurement including electron concentration, electron temperature, and plasma gas temperature. A characteristic curve of carbon dioxide plasma is introduced as a novel outcome, which helps to elucidate the positive impact of applying reduced pressure. 46.4% carbon dioxide conversion efficiency was demonstrated by applying 5 $NL \cdot h^{-1}$ flow rate, 80 mbar, and with 14.5 $MJ \cdot mol^{-1}$ molar energy input utilizing only neat carbon dioxide, and achieved with continuous operation, without using any catalyst, in a straight waveguide system. The results indicate that lowering the pressure enhances the specific power absorption of plasma from the electromagnetic field through electron collisions, which increases the carbon dioxide conversion instead of converting it into heat.

Keywords microwave, carbon dioxide plasma, carbon dioxide conversion

1 Introduction

One of the most important causes of global warming since the beginning of industrialization is the emission of anthropogenic greenhouse gases, from which carbon dioxide plays a key role with the rapidly increasing concentration in the atmosphere reaching 421 ppm on a global annual average in 2023. Achieving net zero carbon emissions by 2050 according to the Paris Agreement is still a significant challenge and an urgent and impactful transition from fossil fuels to more sustainable and environmentally friendly energy sources with restful solutions is necessary. Therefore, carbon capture and storage and carbon capture and utilization technologies [1,2] are gaining increasing interest. The conversion of carbon dioxide into valuable products by utilizing renewable electricity [3] is an attractive method as a way of lowering the carbon footprint and also might play a significant role in terms of creating closed-loop carbon cycles in the future, called carbon dioxide recycling.

Recently, plasma-based carbon dioxide conversion has been considered as an alternative method, as it can operate under mild conditions and can convert fluctuating renewable electricity into value-added products [4,5]. The chemical reactions in plasmas are driven by energetic electrons that provide high densities of electrons, ions, and radicals through electron impact dissociation and excitation, making the plasma highly reactive. The carbon dioxide plasma can be differentiated based on the technique used, common types include dielectric barrier, microwave, glow, radio frequency, and gliding arc discharges [6], from which microwave plasma technology is considered as one of the most promising alternatives [7] because it is electrodeless, cost-effective [8], and scalable making it an optimal plasma source. Qin et al. [6] published a comprehensive review about the status of carbon dioxide conversion by microwave-driven plasmas, including the fundamental mechanism, influence of operating conditions, impact of co-reactants, and utilization of catalysts. The study also highlights some challenges that need to be addressed before scale-up, and

Received February 22, 2025; accepted April 6, 2025; online June 6, 2025

E-mail: zsolt.dobo@uni-miskolc.hu

therefore calls for more research and development within this field. Another review was published by Ong et al. [9], where the carbon dioxide conversion into high-value products by microwave-assisted plasma was thoroughly described. The study also includes the theoretical background, factors that affect the plasma, and the role of catalysts. It was concluded that syngas production should be given more attention in the future as it can serve as a crucial intermediate for different chemicals and clean fuels. Zhu et al. [7] collected and reviewed the various experimental systems focusing on the microwave-assisted carbon dioxide plasmas to provide guidance in selecting an appropriate setup. Wanten et al. [10] summarized the definitions and formulas related to plasma-based carbon dioxide conversion as inconsistencies can be found in reporting the performance metrics across the scientific literature. The above-referenced four reviews give excellent guidelines for microwave-assisted carbon dioxide conversion, highlighting the challenges, difficulties, and opportunities within this field.

The simplest way of creating microwave-assisted carbon dioxide plasma is when the carbon dioxide is utilized in neat form without additives such as a catalyst, while the conversion and energy efficiencies are two major parameters of the process. Wiegers et al. [11] showed 20% carbon dioxide conversion efficiency at 9 standard liters per minute (SLM) carbon dioxide flow rate and 1.4 kW microwave power, utilizing an atmospheric, modular microwave plasma torch. Mitsingas et al. [12] showed a maximum of 9% carbon dioxide conversion efficiency at 48.2 kJ·mol^{-1} molar energy input (MEI) for atmospheric microwave-assisted carbon dioxide plasma. It was highlighted that gas flow rate appears to be the most important parameter affecting both carbon dioxide conversion and energy efficiencies. Typically, decreasing the gas pressure in plasma leads to higher conversions. van Rooij et al. [13] investigated carbon dioxide plasma maintained by microwave. Up to 30% carbon dioxide conversion was reached at around 193 kJ·mol^{-1} MEI, 100 mbar pressure, and 5.00 SLM flow rate, while the conversion rate increased with decreasing the flow rate. Bongers et al. [14] reached a similar conversion efficiency of about 26% carbon dioxide by utilizing a 1 kW magnetron at 164 kJ·mol^{-1} MEI and a reduced pressure of 130 mbar. These studies show that the plasma pressure has a significant influence on conversion efficiency, but also other approaches exist for increasing this parameter including the injection of other gases into the carbon dioxide stream or the usage of catalysts, making the conversion mechanism more complex. Chen et al. [15] highlighted that admixing different gases to carbon dioxide often leads to an increase in carbon dioxide conversion, the relevant studies implement argon, nitrogen, helium, oxygen, or even water. An example is a study performed by Spencer and Gallimore [16], where 10% and 45% carbon dioxide conversion efficiencies were reached at 193 and 2.01 MJ·mol^{-1} MEI, respectively. The flow rate range was 1–16 SLM, while argon was utilized as a mixing agent. The utilization of catalysts also results in elevated carbon dioxide conversion efficiency. The study published by Salden et al. [17] evaluates publications in various ways related to plasma-based carbon dioxide conversion. It can be concluded that the conversion efficiency of around 30%–35% seems as the highest based on 24 publications and 1029 individual data points related to non-catalytic microwave-induced carbon dioxide plasmas. However, the utilization of catalysts can improve the carbon dioxide conversion efficiency by up to 55%, based on 4 publications and 113 individual data points. A reverse vortex configuration combined with a narrow gas inlet is designed by Hecimovic et al. [18] to maximize carbon dioxide conversion by ensuring that the gas fully interacts with the plasma. The gas is then quickly cooled to avoid recombination reactions. The study achieved carbon dioxide conversion rates up to 57% at 900 mbar pressure applying 675.4 kJ·mol^{-1} molar energy. Almost identical results were reported by Kiefer et al. [19] achieving 56.6% conversion at 900 mbar with the cooling channels and reverse vortex setup applying 9808 kJ·mol^{-1} molar energy.

It seems that the highest conversion efficiency and the highest energy efficiency cannot happen at the same time [20]. Based on the study of Salden et al. [17] it can be concluded that most publications depict around 5% and 15% energy efficiencies in cases of microwave-assisted plasma-only and catalytic carbon dioxide conversion, respectively (based on 22 publications and 1193 individual data points). Fuente et al. [21] reported 8% energy efficiency with a flow rate of 0.1–0.2 SLM, 20 mbar pressure, and 150 W introduced microwave power. Chen et al. [22] reported 10% energy efficiency with 675 kJ·mol^{-1} MEI, 2 SLM flow rate, and 40 mbar pressure, using pulsed mode microwave operation with the pulsing frequency of 1.67 kHz. Silva et al. [23] reported 6.4% energy efficiency by mixing 5% nitrogen to the input carbon dioxide, using a tapered waveguide plasma cavity with 2.22 MJ·mol^{-1} MEI. Although the above-mentioned studies show similar results regarding energy efficiency, significantly higher efficiencies are also reported across the literature. D'Isa et al. [20] reported ~35% energy efficiency applying 322.6 kJ·mol^{-1} (10 SLM, 2.4 kW) molar energy. It was also found that the energy efficiency peaks at 120 mbar while the range of investigation was 20–1000 mbar. The "wall-plug" efficiency was found to be 17.9% by Kiefer et al. [19], and energy efficiency of 27% was reported while reaching a conversion of 12.3%. Belov et al. [24] measured 26% energy efficiency with 20 SLM, 2.75 kW introduced microwave power and 200 mbar pressure, in a so called vortex configuration, while Bongers et al. [14] achieved ~50% energy efficiency with 75 SLM, 2.5 kW

introduced microwave power at 200 mbar pressure with a 0.915 GHz microwave system.

Microwave-induced plasma conversion has emerged as a promising method for carbon dioxide dissociation, with various studies examining different operational approaches. Non-catalytic microwave plasmas operated at atmospheric pressure offer straightforward setups and scalability; however, frequent electron-neutral collisions significantly limit their conversion and energy efficiency. Reduced-pressure non-catalytic plasmas mitigate these collisions, improving both conversion and energy efficiencies, although they require additional vacuum equipment and thus more complex control. Catalyst-assisted microwave plasma approaches considerably enhance conversion efficiency and product selectivity through plasma-catalyst synergies but introduce operational complexity because of the microwave system, particularly concerning catalyst stability and cost. Admixture of additional gases, such as argon or nitrogen, into carbon dioxide streams also enhances reaction kinetics and conversion efficiency but similarly complicates the system and reduces energy efficiency. Alternative configurations, including vortex and reverse vortex reactors, achieve high conversion efficiencies by optimizing gas-plasma interactions and rapidly quenching reactions, but their intricate designs demand precise control and their scalability might be challenging. Pulsed microwave plasma operation provides improved energy efficiency and control over plasma parameters through intermittent power delivery but involves increased complexity in power management and measurements. Overall, a fundamental trade-off exists among operational complexity, conversion efficiency, energy efficiency, and scalability. While reduced-pressure non-catalytic microwave plasma systems represent a balanced compromise, catalytic, gas admixture, and advanced reactor configurations offer superior efficiencies at the expense of increased complexity. Selecting an optimal approach thus depends critically on specific application requirements and practical considerations.

Based on the literature, it can be stated that reducing the pressure has a significant positive effect on carbon dioxide conversion and energy efficiency. The main goal of this study is the characterization and optimization of microwave-driven, non-catalyzed neat carbon dioxide plasmas. This was achieved by measuring optical emission spectra and gas composition by gas chromatography under various carbon dioxide flow rates and gas pressures supported by specific model calculations. The degree of carbon dioxide decomposition is also within the focus of the research. The characteristic curve of carbon dioxide plasma is also introduced, published previously only for air plasmas [25].

2 Experimental

The experimental system (Fig. 1) consists of a magnetron and launcher, circulator, water load, 3-stub tuner, directional coupler, and plasma cavity. The introduced

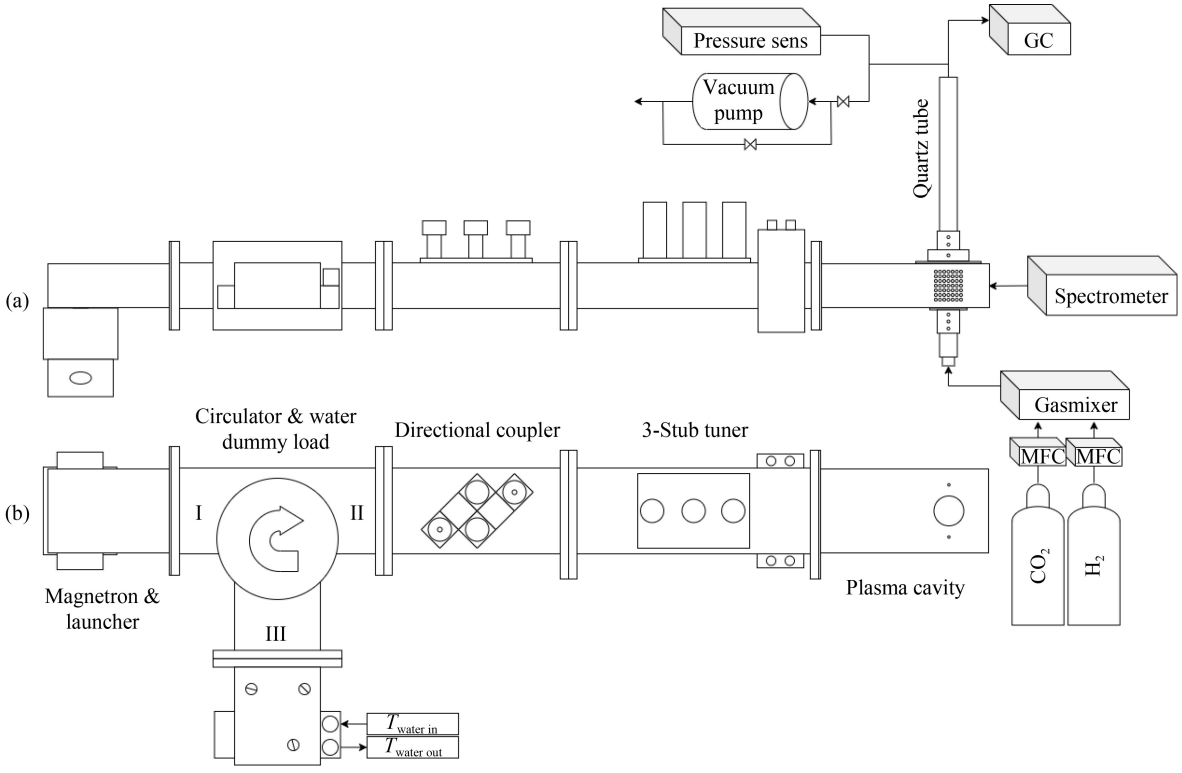

Fig. 1 Schematic diagram of the experimental setup including the equipment utilized: (a) side view; (b) top view.

microwave power was generated with a Toshiba 2M248 type magnetron working at 2.45 GHz rated frequency. The generated microwave power can be continuously adjusted in the interval of 0.2–1 kW. The plasma cavity is a mono-mode waveguide. At the bottom and the top of the plasma cavity, a hole was formed at a distance of $\lambda_g/4$ from its closing plate, where λ_g is the guided wavelength (in our design λ_g = 174 mm [26,27]). A quartz tube is placed into the plasma cavity with the possibility of adjusting its location in axial directions. A nozzle for a gas inlet was placed into the quartz tube, the gas sealing was secured with two rubber O rings. The quartz tube has a 19 mm external diameter, a 16 mm internal diameter, and a 300 mm length. The location of the quartz tube and the nozzle were selected to ensure the highest electric field strength, which was verified by simulation software (Quick Wave v2021:2021.09.10, HN).

The neat carbon dioxide was supplied from a cylinder with a purity of 4.5, while hydrogen had a purity of 5.0. Hydrogen was injected into the carbon dioxide stream only for diagnostic purposes [28,29] during the determination of the plasma characteristics curve at the CO_2:H_2 ratios of 10 and 3 in the cases of atmospheric (1.01 ± 0.02 bar) and reduced (0.43 ± 0.02 bar) pressures, respectively. The flow rates were controlled by mass flow controllers (Sensirion, SFC5500-10SLM). The carbon dioxide and hydrogen gases were premixed before their introduction to the nozzle.

A vacuum pump was utilized to reduce the pressure during the experiments, while the pressure was adjusted by valves as seen in Fig. 1, and it was measured with a pressure transmitter connected to a 4–20 mA measurement device type CALOG-TEMP. The output gas concentration (including carbon dioxide, carbon monoxide, oxygen, and hydrogen) was measured with an Agilent 490 micro GC gas chromatograph (GC) equipped with a CP-COx column.

Before the measurements, the 3-stub tuner was adjusted to form plasma at the lowest possible value of the introduced microwave power, and all measurements were performed with this fixed setup. The carbon dioxide plasma automatically ignited when the pressure reached less than 100 mbar, the applied microwave power was higher than 0.700 kW, and the gas flow rate of 10.0–20.0 NL·h^{-1}. Then, the system was ready to adjust the parameters to the desired levels. All the results were recorded after reaching steady-state conditions, roughly 3 min after the microwave power was applied. The input and product gases used for measurements were in laboratory conditions. All the pressure values reported in this study represent absolute pressure.

Optical emission spectra (OES) was taken through the inspection holes of the plasma cavity (Fig. 1). The fiber optic cable was connected to an HR4PRO-XR-ES type spectrometer that performed measurements in the ~200–1100 nm wavelength range with a resolution of 0.25 nm. Each OES recording is the average of five measurements. The averaging time of the spectrometer was set manually so that the spectral peak of interest with the highest intensity value for each recording was as close as possible to the maximum intensity value that the spectrometer could record without saturation. All the OES were normalized while processing the measured data according to the spectrometer's averaging time, and the baseline of the spectrum of interest was also removed during the evaluation.

The calculation of the electron number density was based on the Stark broadening of the atomic H_α (hydrogen alpha) lines using the optical emission spectrum recordings. The extended Voigt function was fitted to the measured relative intensities (I_V, –, normalized to unity) of the H_α part of the optical emission spectrum, as [30]:

$$I_V = Ae^{-\left(\frac{x-x_0}{2\sigma}\right)} + \frac{1-A}{1+\left(\frac{x-x_0}{\gamma}\right)^2}, \tag{1a}$$

where A (–), σ (nm), and γ (nm) are fitting constants, x (nm) is the wavelength of the measured carbon dioxide plasma, x_0 = 656.17 nm is the wavelength of the H_α characteristic peak. Once the values of the three fitting parameters are found, parameter a (nm) can be estimated from the following equality (where a is half of the full width half area):

$$\frac{1}{2} = \frac{\int_{x_0-a}^{x_0+a} I_V \mathrm{d}x}{\int_{-\infty}^{+\infty} I_V \mathrm{d}x}. \tag{1b}$$

Then, the electron number density n_e (m^{-3}) can be calculated as [31]:

$$n_e = 10^{23}\left(\frac{a}{0.550}\right)^{1.47}. \tag{1c}$$

Equation (1c) was first reported by Gigosos et al. [32], and corrected later by Konjević et al. [31] (note: the numbers of digits of parameters in Eq. (1c) are simplified to 3 reasonable digits by us).

Electron temperature (T_e, K) is another crucial parameter of the electron. Atomic oxygen emission lines were used to obtain the excitation temperature (T_{ex}, K), which is a lower estimate of the electron temperature ($T_{ex} \leqslant T_e$) [25,33]. Because of the difficulties of measuring the electron temperature, $T_{ex} \cong T_e$ approximation is used here, as a good alternative [34]. The following equation describes the spectral intensity (I_{ij}, –) of atomic oxygen from its excited level of i to the ground level j, following the Boltzmann energy distribution:

$$I_{ij} = g_i \frac{A_{ij}}{\lambda_{ij}} \exp\left(-\frac{E_i}{k_B T_{ex}}\right), \tag{2a}$$

where g_i (–) is the degeneracy of level i, A_{ij} (s^{-1}) is the Einstein coefficient for the electronic transition from level i to j, λ_{ij} (nm) are the characteristic wavelengths for atomic oxygen collected in Table 1, E_i (J) is the energy at

excited level i, k_B (= 1.381 × 10^{-23} J·K^{-1}) is the Boltzmann constant. After I_{ij} is measured at λ_{ij}, the values of g_i, A_{ij}, and E_i are taken from Table 1 and the values are plotted in coordinates of $\ln[(I_{ij}\lambda_{ij})/(g_iA_{ij})]$ as a function of E_i. The slope of the fitted straight line equals $-1/(k_B \times T_{ex})$ from Eq. (2a). The value of T_{ex} is calculated from this slope [25,33,35] and from here $T_{ex} \cong T_e$ follows [35].

The rotational temperature (T_{rot}, K) of the OH radical is also calculated using the Boltzmann plot method on the spectral peaks between 306 and 316 nm to determine the typical temperature of the plasma. This belongs to the $A^2\sum^+ \rightarrow X^2\prod_\gamma$ electron transition of the OH radical [37–39], which temperature is roughly the same as the plasma gas temperature (T_g, K) [40]. Equation (2b) was used to perform the calculation [39], which applies to case b out of Hund's cases to the OH radical, according to which the intensity of the spectrum line ($I_{K'K''}$, –) is [39]:

$$I_{K'K''} = C\left(2K' + 1\right)\frac{A_{K'K''}}{\lambda_{K'K''}}\exp\left(-\frac{E_{K'}}{k_B T_{rot}}\right), \qquad (2b)$$

where C (–) is a constant, $A_{K'K''}$ (–) is the rotational transition probability, $\lambda_{K'K''}$ (nm) is the wavelength of the $A^2\sum^+ \rightarrow X^2\prod_\gamma$ electron transition, K' and K'' (–) represent upper and lower rotational levels, respectively, $E_{K'}$ (J) is the energy of the upper rotational level. The $A_{K'K''}$ and $E_{K'}$ values were determined based on Dieke and Crosswhite's spectrum simulation and high-precision measurements [41], which were refined by Chidsey et al. [42]. The values used for the calculations are summarized in Table 2. Plotting the values of $\ln[(I_{K'K''}\lambda_{K'K''})/((2K' + 1)A_{K'K''})]$ as a function of $E_{K'}$, the slope of the line fitted to the points is equal to $-1/(k_B \times T_{rot})$, from where $T_{rot} \cong T_g$ can be calculated.

Table 1 Values used for the calculation of electron temperature [35,36]

λ_{ij}/nm	g_i	E_i/(10^{-18} J)	A_{ij}/(10^7 s^{-1})
715.67	5	2.3167	5.05
777.34	15	1.7207	3.69
844.65	9	1.7608	3.22

Table 2 Values used for the calculation of the rotational temperature of the OH radical [39,41,42]

$\lambda_{K'K''}$ /nm	Branch	K'	$E_{K'}$ /(10^{-19} J)	$A_{K'K''}$
306.3565	R1	10	6.8101	314
306.9177	R2	8	6.6845	316
309.2394	Q1	8	6.6848	739
309.5342	Q1	9	6.7443	734
310.5663	Q2	11	6.8816	722
313.0276	P1	9	6.7443	421
313.4339	P2	9	6.7439	410
314.0731	P2	10	6.8097	401
315.4507	P2	12	6.9597	380
315.8507	P1	13	7.0443	369
316.1892	P2	13	7.0437	368
316.6336	P1	14	7.1343	355

From the calculated gas temperatures, the neutral particle density (n_{np}, m^{-3}) can be estimated using the ideal gas law, expressed as [43]:

$$n_{np} \cong \frac{p}{k_B T_g}, \qquad (3)$$

where p (Pa) is the gas pressure. The ion density (n_i, m^{-3}) is lower by two orders of magnitude compared to n_{np}, that is why n_i is neglected in Eq. (3).

The total electron collisional cross section (σ_{tot}, m^2) was found by us by using the data from the literature (see Fig. 2 [44–47]) as a function of electron temperature explained above.

The velocity of the neutral particles and the ions is neglected compared to the much larger velocity of the electrons (v, m·s^{-1}) written using their thermal velocity [48]:

$$v = \sqrt{\frac{8T_e k_B}{\pi m_e}}, \qquad (4)$$

where m_e = 9.109 × 10^{-31} kg is the electron mass. The electron-neutral particle collision frequency ($\nu_{e\text{-}np}$, s^{-1}) can be calculated with the parameters explained above [49]:

$$\nu_{e-np} = n_{np} v \sigma_{tot}. \qquad (5)$$

The microwave-induced plasmas are collision-dominated non-thermal plasmas [50]. Their specific absorbed power due to collisions ($\mathcal{P}_{coll}$, W·(m^{-3}·(V·m^{-1})$^{-2}$) is given as [48,49,51]:

$$\mathcal{P}_{coll} \equiv \frac{P_\omega}{VE^2} = \frac{e^2}{m_e} n_e \frac{\nu_{e-np}/\omega}{1 + (\nu_{e-np}/\omega)^2}, \qquad (6)$$

where P_ω (W) is the power absorbed by the plasma, ω (s^{-1}) is the angular frequency of the introduced microwave power of the magnetron frequency of f_{MW} =

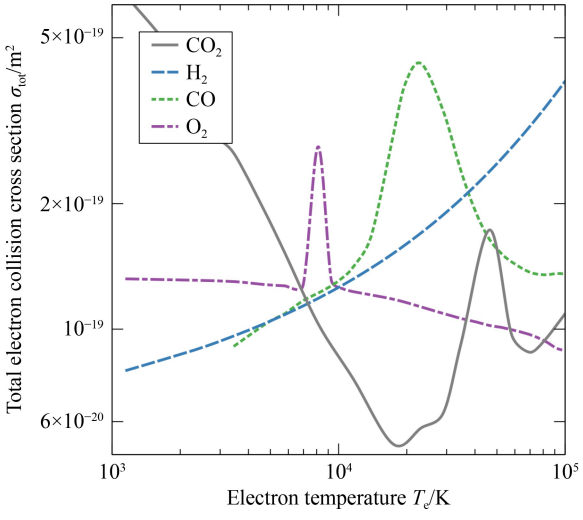

Fig. 2 Total electron collision cross section as a function of electron temperature in the cases of carbon dioxide [44], carbon monoxide [45], hydrogen [46], and oxygen [47] molecules.

2.45 GHz ($\omega = 2\pi f_{MW} = 1.54 \times 10^{10}$), $e = 1.602 \times 10^{-19}$ C is the charge of the electron, V (m^3) is the plasma gas volume, E ($V \cdot m^{-1}$) is the electric field strength in the plasma cavity. The conversion of carbon dioxide takes place according to the following reaction [10,52] with its standard molar reaction enthalpy:

$$CO_2 \rightarrow CO + \frac{1}{2}O_2, \Delta H^0 = 283 \frac{kJ}{mol\text{-}CO_2} = 283 \frac{kJ}{mol\text{-}CO}. \quad (7)$$

The conversion efficiency of carbon dioxide (χ_{CO_2}, %) is defined as:

$$\chi_{CO_2} \equiv 100 \frac{n^0_{CO_2} - n_{CO_2}}{n^0_{CO_2}}, \quad (8)$$

where $n^0_{CO_2}$ (mol) is the amount of carbon dioxide molecules in the input gas and n_{CO_2} (mol) is the same in the output gas after passing the plasma. The volume ratio of carbon monoxide is measured in the output gas (y_{CO}, $m^3 \cdot m^{-3}$) with a GC. From its measured value, the conversion efficiency of carbon dioxide is calculated as [10]:

$$\chi_{CO_2} = 100 \frac{y_{CO}}{1 - 0.5 y_{CO}}. \quad (9)$$

The molar energy input, MEI (E_m, $J \cdot mol\text{-}CO_2^{-1}$) of the microwave power per unit amount of introduced CO_2 gas can be calculated with the following formula [10]:

$$E_m = 80640 \frac{P_{MW}}{Q_{gas}}, \quad (10)$$

where P_{MW} (W) is the introduced microwave power, Q_{gas} ($NL \cdot h^{-1}$) is the introduced carbon dioxide flow rate, while $80640 = 3600\ s \cdot h^{-1} \times 22.4\ NL \cdot mol^{-1}$. Then, the conversion energy efficiency of carbon dioxide according to Eq. (7) (η_{CO_2}, %) can be determined as [10]:

$$\eta_{CO_2} = \frac{\chi_{CO_2} \Delta H^0}{E_m}. \quad (11)$$

The degree of ionization (χ_i, –) is defined as the ratio of the amount of ions in the plasma to the total amount of the particles in the same [51]:

$$\chi_i \equiv \frac{n_i}{n_{np} + n_i}, \quad (12)$$

where n_i (m^{-3}) is the ion density.

The degree of ionization ranges from complete ionized fusion plasmas ($\chi_i \approx 1$) to technical or laboratory plasmas ($\chi_i \approx 10^{-6} \ldots 10^{-2}$). The critical degree of ionization, above which a gas becomes a plasma varies between different types of plasma and may be as little as 10^{-6} [33,53].

3 Results and discussion

3.1 The primary experimental results and the primary derived values

In columns 2–5 of Table 3, the experimental conditions of our 15 experiments are collected. In the top Fig. 3 examples of the recorded optical emission spectra are shown for atmospheric and reduced pressures. The enlarged parts of the spectra are shown for OH, H_α, and atomic O in the three bottom plots in Fig. 3. These enlarged spectra were used to create Figs. 4(a)–4(c). Part of our measured OES around the H_α peak is shown in Fig. 3(a) for experiment 1 of Table 3, as an example. The fitting parameters for the Voigt function of Eq. (1a) for this first experiment were found as: A = 0.268, σ = 0.279 nm, and γ = 0.169 nm. From here, a = 0.177 nm was found. Substituting this value into Eq. (1c) n_e = 1.88×10^{22} m^{-3} is obtained (see column 6 of Table 3). Other values in column 6 of Table 3 were found in a similar way.

The electron temperature was estimated using figures such as Fig. 3(b) given as an example for experiment 1 of Table 3. From the slope of the curve using the Boltzmann

Table 3 The primary experimental parameters[a] and the primary derived parameters[b]

No.	$p \pm 0.02$/bar	CO_2/($NL \cdot h^{-1}$)	H_2/($NL \cdot h^{-1}$)	P_{MW}/kW	($n_e \pm 0.1$)/(10^{22} m^{-3})	($T_e \pm 2\%$)/kK	($T_g \pm 0.09$)/kK
1	1.01	15.0	1.50	0.8	1.88	13.7	2.94
2	1.01	20.0	2.00	0.9	2.01	16.6	2.97
3	1.01	25.0	2.50	0.9	1.80	14.7	2.91
4	1.01	30.0	3.00	0.9	1.97	14.4	2.92
5	1.01	35.0	3.50	0.9	2.06	16.1	2.84
6	1.01	40.0	4.00	0.9	1.97	14.0	2.85
7	1.01	45.0	4.50	1.0	1.94	14.6	2.87
8	0.430	15.0	5.00	0.8	2.19	11.0	3.00
9	0.430	15.0	5.00	1.0	1.80	13.3	3.10
10	0.430	20.0	6.67	0.8	2.08	13.2	2.93
11	0.430	20.0	6.67	1.0	2.20	15.0	2.84
12	0.430	25.0	8.33	0.9	2.47	9.90	2.95
13	0.430	25.0	8.33	1.0	2.38	8.40	2.96
14	0.430	30.0	10.0	0.8	2.43	6.60	3.04
15	0.430	30.0	10.0	0.9	2.44	6.30	3.18

a) Columns 2–5; b) last 3 columns: the electron number density n_e, the electron temperature T_e, and the plasma temperature T_g.

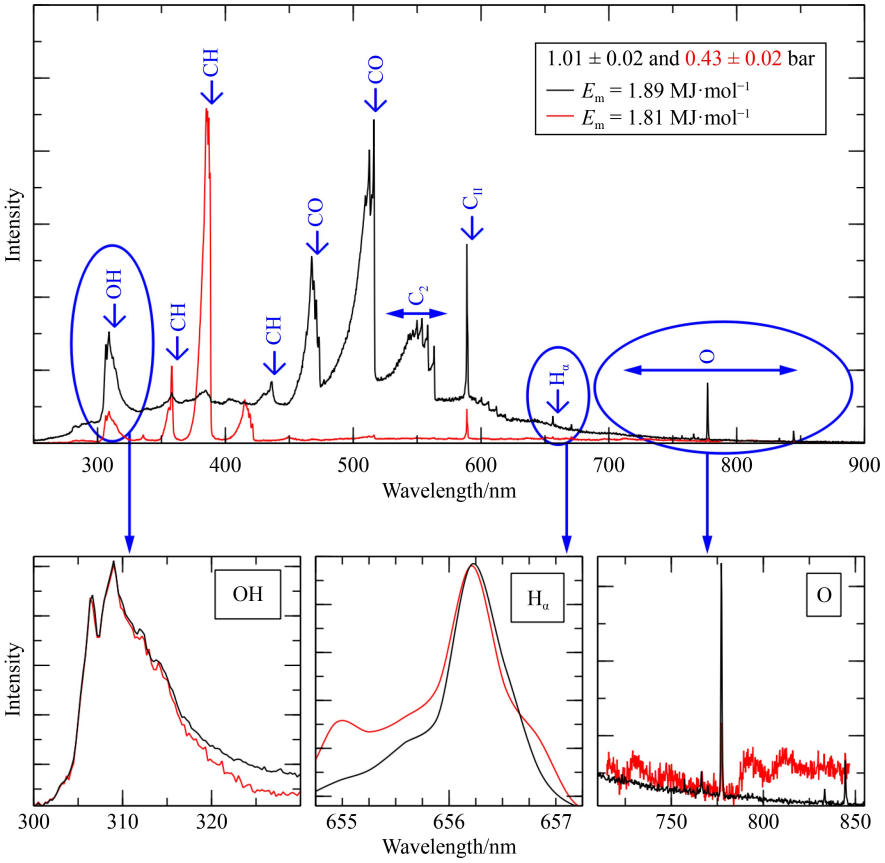

Fig. 3 OES recordings at atmospheric and reduced pressures in almost identical molar energy input values calculated by Eq. (10).

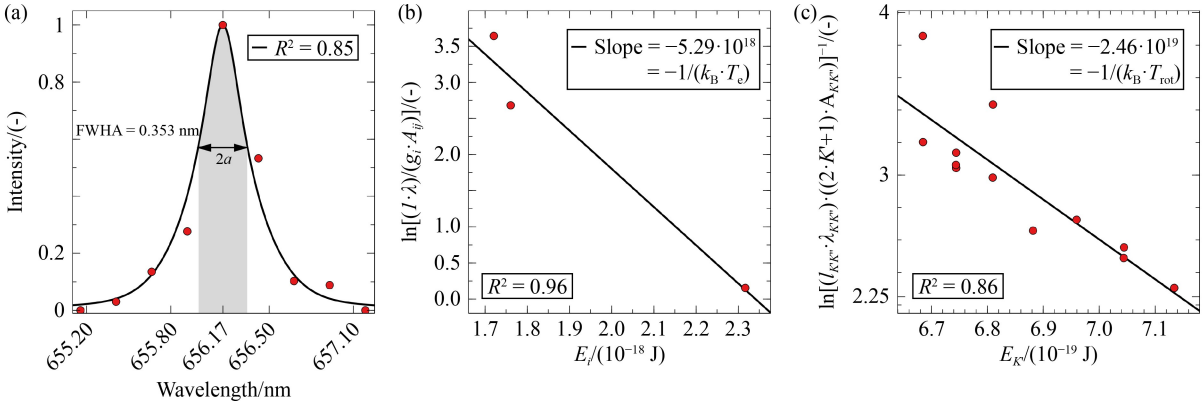

Fig. 4 Example of experimental results for experiment 1 in Table 3 measured at 15.0 NL·h^{-1} carbon dioxide, 1.50 NL·h^{-1} H_2, 0.800 kW microwave power at atmospheric pressure: (a) the H_α peak used to estimate the FWHA utilizing observed in OES; (b) and (c) are the Boltzmann plots to estimate the electron temperature and the plasma gas temperature, respectively.

constant the electron temperature is found as: $T_e \cong$ 13.7 kK (see column 7 of Table 3). The plasma gas temperature was estimated using figures such as Fig. 3(c) given as an example for experiment 1 of Table 3. From the slope of the curve using the Boltzmann constant the plasma gas temperature is found as: $T_g \cong$ 2.94 kK (see column 8 of Table 3). Other values in columns 7 and 8 of Table 3 were found in a similar way.

The calculated electron number density ranges from 1.80 to 2.06 (× 10^{22} m^{-3}) for atmospheric pressure and from 1.80 to 2.47 (× 10^{22} m^{-3}) for reduced pressure, respectively. One can see that these results overlap with no clear influence of the gas pressure on the electron density in the plasma. In most cases, the electron number density is in the range of 10^{16}–10^{21} m^{-3} [15]. Yubero et al. [54] measured (4–5) × 10^{21} m^{-3}. de la Fuente et al. [21,29] measured (0.53–2.3) × 10^{21} m^{-3} using Gigosos's method [32] and (1.9–7.3) × 10^{21} m^{-3} using Laux's method [55], by applying Voigt profile to H_β spectrum. Zhang et al. [56] measured 3.3 × 10^{23} m^{-3} using Mach–Zehnder interferometer by applying 1 kW microwave power and concluded that this is one order of

magnitude higher compared to that obtained from the Stark broadening of spectral lines. Based on the articles above our measured electron number density shows higher numbers but this is not unprecedented in the literature.

The electron temperatures range from 13.7 to 16.6 kK at atmospheric pressure and from 6.30 to 15.0 kK at reduced pressure, respectively, which fits in the range given in other papers [9,15,21,29]. Although these ranges also overlap, here we can conclude that decreasing the plasma gas pressure leads to reduced electron temperatures. This is probably due to the increased coupling efficiency of the plasma (see below for more details).

The plasma gas temperature ranges from 2.84 to 2.97 kK and from 2.84 to 3.18 kK at atmospheric and reduced pressures, respectively. Although these values mostly overlap, one can conclude that decreasing the plasma gas pressure leads to a small increase in the plasma gas temperature. Based on [7,9,15,57] review papers our determined plasma gas temperatures agree with the literature. Snoeckx and Bogaerts [5] published a detailed carbon dioxide plasma review, where slightly lower numbers are presented with the gas temperature in the order of 2 kK. There are more common methods in recent papers to determine the plasma gas temperature, based mostly on the OH radical [40,58,59] and the C_2 Swan band [40,60]. These two methods were found as a good temperature determination in the case of microwave-induced plasmas, however, it can also be concluded that the case of C_2 Swan band is insensitive to external plasma parameters such as introduced microwave power and flow rate [60], and the spectral analysis of C_2 Swan band shows higher temperatures. Under atmospheric pressure, plasma tends to have a central hot core, whereas, at reduced pressure, the plasma becomes more diffuse [6,9,61]. It is possible to reach temperatures of 3–7 kK in the central core [20,62,63] without melting the quartz tube, which has a softening temperature of approximately 1.80 kK [64]. However, under reduced pressure, where the plasma comes into contact with the quartz tube walls, a gas temperature range of 2–3 kK is more plausible. Along with this, the literature indicates that there is not a significant difference in gas temperature between atmospheric and reduced pressure conditions.

3.2 The characteristic curve of the carbon dioxide plasma gas

The microwave power absorption by collision between electrons and neutral particles in the plasma gas ($\mathcal{P}_{\text{coll}}$) was calculated by Eqs. (3–6) and Fig. 2 (see Table 4). One can see that the values of $\mathcal{P}_{\text{coll}}$ significantly increased with decreasing the plasma gas pressure. As follows from Eq. (6) and Table 4, this is mostly due to the decreased frequencies of electron-neutral-particle collisions, being a larger effect compared to the reduced density of neutral particles.

Equation (6) was used to plot Fig. 5, using the average value of electron density from Table 3. Figure 5 is called here the characteristic curve of the carbon dioxide plasmas. One can see that Fig. 5 passes through a maximum point at $\nu_{\text{e-np}}/\omega = 1$, denoted as $\mathcal{P}_{\text{coll}}^{\max}$. This is because at $\nu_{\text{e-np}}/\omega = 1$ the electrons can absorb the highest amount of energy from the electromagnetic field in the time period between two collisions. From Fig. 5, the value of $\mathcal{P}_{\text{coll}}^{\max} = 19.5\ \text{kW}\cdot\text{V}^{-2}\cdot\text{m}^{-1}$ is valid for the carbon dioxide plasma. Based on this, a new quantity called here the "coupling efficiency of the microwave with the plasma gas" is introduced, denoted as η_{coupling} and defined as:

$$\eta_{\text{coupling}} \equiv 100\frac{\mathcal{P}_{\text{coll}}}{\mathcal{P}_{\text{coll}}^{\max}}. \tag{13}$$

The coupling efficiency calculated by Eq. (13) is shown Table 4 and is plotted along the right-hand side y-axes of Fig. 5. Based on the characteristic curve shown in Fig. 5,

Table 4 Further parameters of 15 carbon dioxide plasma experiments (see Table 3) calculated by Eqs. (3–6, 12, and 13) and Fig. 2

No	$p \pm 0.02$/bar	$\sigma_{\text{tot}}/(10^{-20}\ \text{m}^2)$	$(n_{\text{np}} \pm 2\%)/(10^{24}\ \text{m}^{-3})$	$(\nu \pm 2\%)/(10^5\ \text{m}\cdot\text{s}^{-1})$	$(\nu_{\text{e-np}} \pm 5\%)/(10^{10}\ \text{s}^{-1})$	$(\mathcal{P}_{\text{coll}} \pm 5\%)/(\text{kW}\cdot\text{V}^{-2}\cdot\text{m}^{-1})$	$\eta_{\text{coupling}}/\%$	$(\chi_i \pm 5\%)/10^{-2}$
1	1.01	7.20	2.45	7.27	12.8	4.10	21.0	0.760
2	1.01	6.41	2.44	7.99	12.5	4.50	23.1	0.816
3	1.01	6.84	2.49	7.54	12.8	3.94	20.2	0.719
4	1.01	6.96	2.48	7.45	12.9	4.30	22.1	0.788
5	1.01	6.50	2.55	7.87	13.1	4.42	22.7	0.800
6	1.01	7.09	2.55	7.35	13.3	4.17	21.4	0.768
7	1.01	6.88	2.52	7.51	13.0	4.18	21.4	0.763
8	0.430	9.82	1.01	6.51	6.42	9.16	47.0	2.12
9	0.430	9.22	0.97	7.15	6.39	7.57	38.8	1.82
10	0.430	9.23	1.06	7.15	6.98	8.09	41.5	1.93
11	0.430	8.76	1.09	7.62	7.30	8.19	42.0	1.97
12	0.430	10.2	1.09	6.20	6.88	9.70	49.8	2.21
13	0.430	11.4	1.09	5.69	7.06	9.14	46.9	2.13
14	0.430	12.8	1.08	5.05	6.96	9.48	48.6	2.20
15	0.430	13.0	1.04	4.95	6.65	9.93	50.9	2.30

it can be concluded, that in the case of atmospheric pressure conditions, the carbon dioxide plasma is weakly coupled ($\eta_{coupling}$ = 21.7% in average), while at reduced pressure the coupling efficiency is significantly increased ($\eta_{coupling}$ = 45.7% in average). Using Fig. 5, the following two optimum cases can be estimated: (1) The optimum magnetron frequency is estimated to be about 20 GHz, corresponding to the atmospheric pressure of the carbon dioxide plasma gas; (2) keeping the magnetron frequency at the value of 2.45 GHz, the optimum pressure of the carbon dioxide plasma gas is estimated to have a magnitude of 0.1 bar. The characteristic curve of the carbon dioxide plasma presented here is considered as a novel approach for describing carbon dioxide plasmas, as previous, non-carbon dioxide related studies present characteristic curves only in the case of air plasmas [25].

Figure 6 shows the dependence of the degree of ionization on the specific power absorption by collision using the data presented in Table 4. One can see a good linear correlation for both pressure values used by us. It means that the electron-neutral particle collisions effectively lead to the formation of new free electrons, i.e. to the ionization of the plasma gas. In other words, the part of the introduced microwave power that is absorbed by the electron-neutral particle collisions is mostly used for its ionization. It is also clear from Fig. 6 that by decreasing the pressure of the plasma gas, both the specific power absorption and the degree of ionization increase proportionally. However, as follows from the semi-empirical equations shown in Fig. 6, the semi-empirical coefficient differs only by about 28% when the pressure is reduced by more than twice.

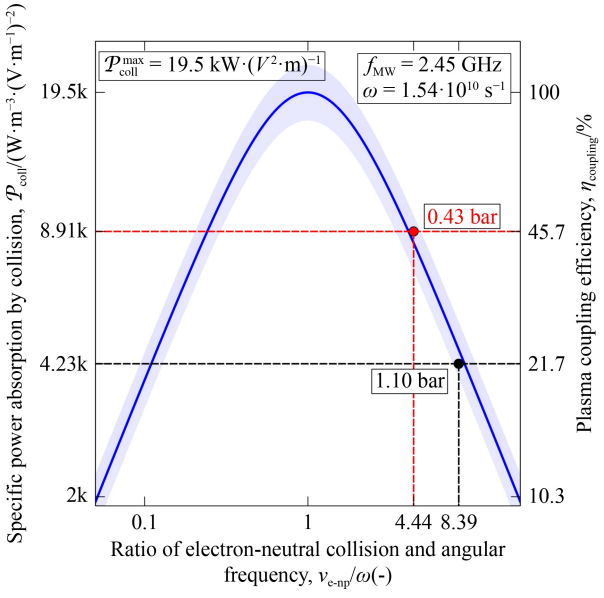

Fig. 5 The log-log graph of specific power absorption by collision of electrons and neutral particles as a function of the ratio of electron-neutral collisional frequency and the microwave source angular frequency valid for two pressures: this is the characteristic curve of the carbon dioxide plasma introduced here and calculated by Eq. (6) at the average values of n_e taken from the 15 measured-calculated values of column 6 of Table 3. The two points are average measured-calculated points from Table 4 at atmospheric and reduced pressures.

3.3 Carbon dioxide conversion- and energy efficiency

After the characterization of the carbon dioxide plasma presented in the previous sub-sections, in this sub-section new measurements were performed utilizing pure carbon dioxide (without hydrogen-addition used above only for diagnostic purposes). In Table S1 (cf. Electronic Supplementary Material, ESM) the fixed technological parameters for each experiment are collected in columns 2–4. The major measured quantity was the concentration of the carbon monoxide gas (see column 5 of Table S1 (cf. ESM)). The conversion efficiency of carbon dioxide was calculated by Eq. (9) and the values are given in column 6 of Table S1. The molar energy input of the microwave power per unit amount of introduced carbon dioxide gas was calculated by Eq. (10) and the values are given in column 7 of Table S1 (cf. ESM). The conversion energy efficiency of carbon dioxide was calculated by Eq. (11) and the values are given in column 8 of Table S1 (cf. ESM).

In the top plots of Fig. 7, the carbon dioxide conversion efficiency and energy efficiency as a function of molar energy input at different flow rates and reduced pressures are shown. One can see approximately opposite trends of the two parameters. Some increase (or saturation) in the carbon dioxide conversion efficiency is found with increasing the molar energy input by the microwave.

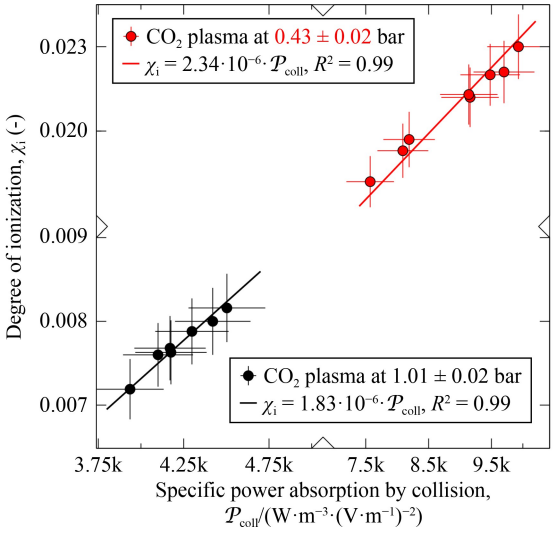

Fig. 6 The degree of ionization of the carbon dioxide plasma as a function of the power absorption by collision between electrons and neutral particles taken from Table 4 in cases of atmospheric pressure (see left bottom black data points) and reduced pressure (see right top red data points). Note that both the *x*-axes and the *y*-axes are broken to show the atmospheric and reduced pressure data in the same graph.

However, the conversion energy efficiency of carbon dioxide monotonically decreases with increasing the molar energy input. It seems that both efficiencies cannot be increased at the same time at a fixed pressure. As our goal is to find the complex optimum of the efficiencies, in the bottom plots of Fig. 7, the product of these two efficiencies ($\chi_{CO_2} \cdot \eta_{CO_2}$) is shown as a function of molar energy input. One can see that in one out of three bottom figures, a maximum point is found around MEI ≅ 1.10 MJ·mol^{-1} for the experiments with 60.0 NL·h^{-1} carbon dioxide and at 0.097 bar, considered as an optimum point of operation. However, in the other two figures, no maxima are found within the range of operations of stable carbon dioxide plasma, although the increasing trends in $\chi_{CO_2} \cdot \eta_{CO_2}$ values can be seen.

Figure 8(a) shows the carbon dioxide conversion efficiency as a function of the energy efficiency at different carbon dioxide flow rates and pressures, but with fixed microwave power values. The results indicate that the carbon dioxide conversion efficiency, and also the energy efficiency increase by decreasing the pressure, which agrees with the literature [12,13]. It can be also seen in Fig. 8a that the conversion efficiency is higher at atmospheric pressure conditions with a higher flow rate,

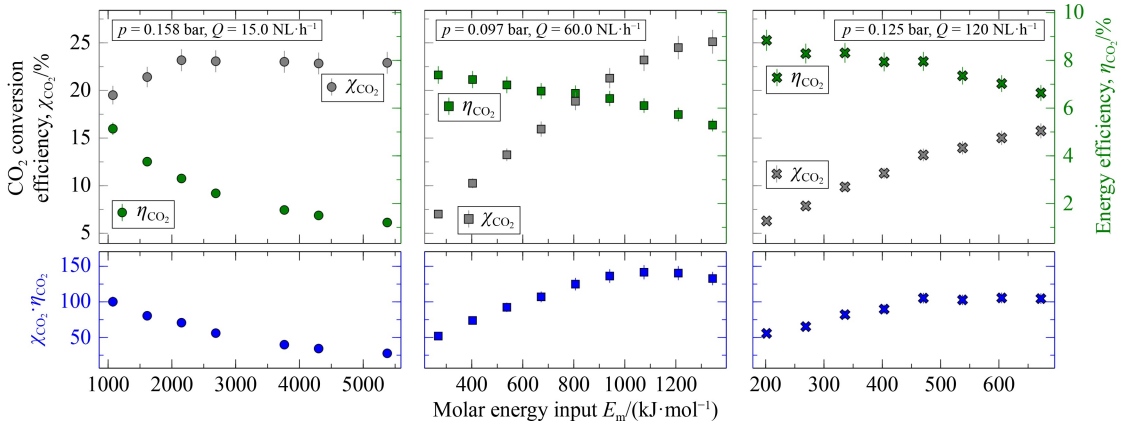

Fig. 7 Carbon dioxide conversion efficiency and energy efficiency (top figures) and their product (bottom figures) as a function of molar energy input at different flow rates and reduced pressures (the left figures are valid at 15.0 NL·h^{-1} and 0.158 bar, the middle figures are valid at 60 NL·h^{-1} and 0.097 bar, and the right figures are valid at 120 NL·h^{-1} and 0.125 bar).

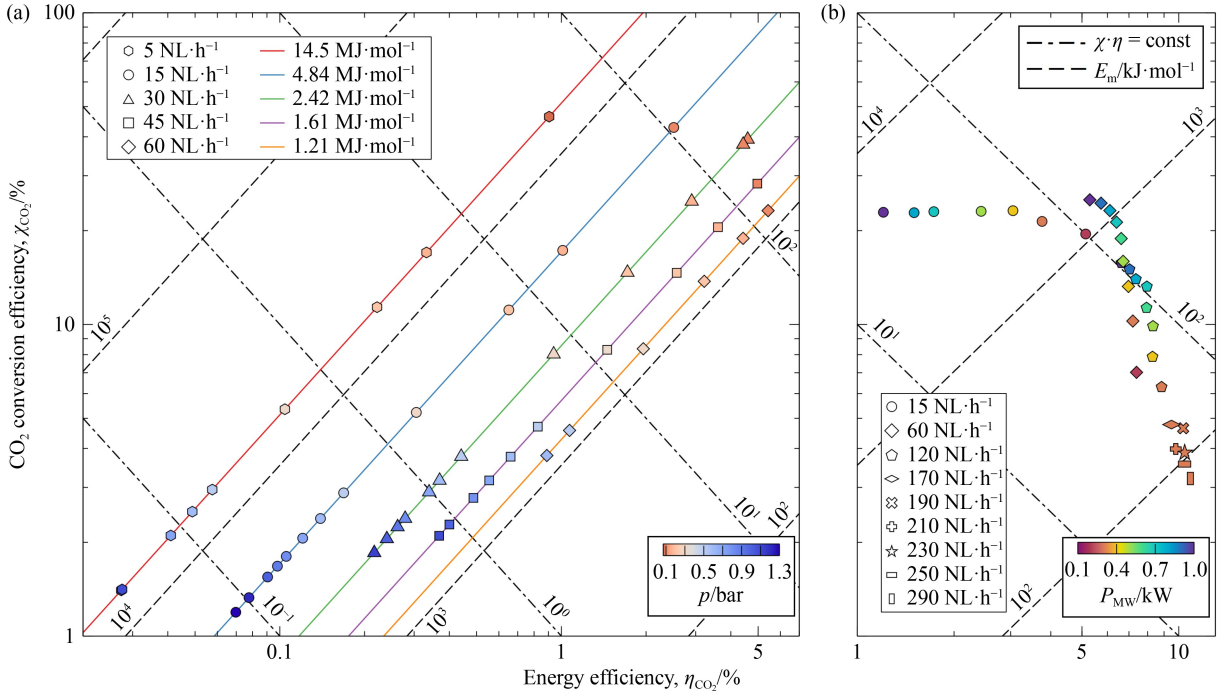

Fig. 8 Carbon dioxide conversion efficiency as a function of energy efficiency. (a) The data points were taken at different pressures and carbon dioxide flow rates. The microwave power is fixed at 0.9 kW, the color bar represents the applied pressure. The molar energy input is also shown in the legend for better comparison. (b) The data points were taken at different microwave power values and carbon dioxide flow rates. The pressure is fixed at 131 ± 25 mbar, the color bar represents the input microwave power.

but this turns to the opposite at low pressure (~0.08 bar), where the measurements show higher conversion efficiency at a lower flow rate. In general, energy efficiency tends to increase by increasing the carbon dioxide flow rate as it intensifies the number of carbon dioxide molecules passing through the plasma cavity. Figure 8(b) gives a summary of the carbon dioxide conversion efficiency as a function of energy efficiency at various microwave powers and carbon dioxide flow rates at fixed values of plasma pressure. The energy efficiency can be intensified by increasing the carbon dioxide flow rate, but at the same time, the conversion efficiency significantly decreases if the pressure and the microwave power are fixed. At flow rates of 170 $NL \cdot h^{-1}$ or higher, only single measurement points are available, because any further reduction in microwave power resulted in the loss of the plasma. Based on this plot it can be concluded that a relatively constant carbon dioxide conversion value can be reached up to the energy efficiency of 6%–7% and up to 120 $NL \cdot h^{-1}$. The carbon dioxide conversion efficiency tends to have a relatively constant value, especially in the case of 15 $NL \cdot h^{-1}$, which might be the result of saturation. Further increasing the energy efficiency (i.e., above 6%–7%) is possible, but a significant reduction in carbon dioxide conversion occurs. A good example is the case of 60.0 $NL \cdot h^{-1}$, where the carbon dioxide conversion efficiency tends to significantly decrease by decreasing the input microwave power.

The highest measured energy efficiency of 10.9 ± 0.5% was determined with 0.834 $MJ \cdot mol^{-1}$ energy input and 290 $NL \cdot h^{-1}$ flow rate of pure carbon dioxide (Fig. 8(b)). This was achieved with continuous operation, without using any catalyst, in a straight waveguide system. On the other side, only 3.2% of carbon dioxide conversion efficiency was measured by applying the same settings. In contrast, the highest carbon dioxide conversion efficiency of 46.4 ± 2.3% was measured by applying 80.0 mbar and 5.00 $NL \cdot h^{-1}$ flow rate, with 14.5 $MJ \cdot mol^{-1}$ energy input. This conversion efficiency is relatively high compared to other values reported elsewhere [13,14,17]. An optimal operating condition can be identified at a flow rate of 30 $NL \cdot h^{-1}$, molar energy input of 2.42 $MJ \cdot mol^{-1}$, and the lowest examined pressure where the product of conversion and energy efficiency is the highest. The plot seen in Fig. 8(a) suggests that the carbon dioxide conversion efficiency might be further enhanced by further decreasing the pressure of the plasma gas, which also might influence positively the energy efficiency. As was discussed in sub-sections 3.1 and 3.2, the power absorption roughly doubles under reduced pressure compared to atmospheric pressure (Fig. 4), while the plasma gas temperature remains relatively constant (2.84–2.97 kK at atmospheric pressure, and 2.84–3.18 kK at reduced pressure). This increased power absorption can be attributed to the increased yield of the endothermic reaction, due to increased carbon dioxide conversion.

4 Conclusions

The characteristic curve of carbon dioxide plasma was introduced. Calculations were corroborated by optical emission spectroscopy measurements, from which the plasma gas temperature, electron density, and electron temperature were determined. The characteristic curve is useful in system design, particularly for estimating the coupling quality and specific power absorption by collision at generally available microwave frequencies (0.915, 2.45, and 5.8 GHz). It can be determined by examining the plasma characteristic curve, whether pressure reduction is necessary, considering the associated investment and operating costs. The optimal microwave frequency of 20 GHz was estimated corresponding to the atmospheric pressure using the characteristic curve, while with the 2.45 GHz microwave frequency (used in this paper) the optimal pressure was estimated in the magnitude of 0.1 bar. Additionally, the degree of ionization was found to increase linearly with the specific power absorbed through collisions.

Reducing the pressure in the carbon dioxide plasma enhances its ability to absorb power from the microwave field, generated by a 2.45 GHz magnetron through electron collisions, thereby increasing carbon dioxide conversion instead of plasma gas temperature. The highest recorded neat carbon dioxide conversion efficiency was 46.4 ± 2.3% in a continuous, catalyst-free operation using a straight waveguide system, while the peak energy efficiency of 10.9 ± 0.5% was measured. These results reveal that microwave-induced carbon dioxide plasma shows a promising approach on a way of producing value-added products.

Competing interests The authors declare that they have no competing interests.

Acknowledgement The project has been implemented with the support provided by the Ministry of Culture and Innovation of Hungary from the National Research, Development and Innovation Fund, financed under the 2020-1.1.2-PIACI-KFI-2020-00074 funding scheme.

Funding Note Open access funding provided by University of Miskolc

References

1. Al-Mamoori A, Krishnamurthy A, Rownaghi A A, Rezaei F. Carbon capture and utilization update. Energy Technology, 2017, 5(6): 834–849
2. Baena-Moreno F M, Rodríguez-Galán M, Vega F, Alonso-Fariñas B, Vilches Arenas L F, Navarrete B. Carbon capture and utilization technologies: a literature review and recent advances. Energy Sources Part A: Recovery, Utilization, and Environmental Effects, 2019, 41(12): 1403–1433
3. Koytsoumpa E I, Bergins C, Buddenberg T, Wu S, Sigurbjörnsson Ó, Tran K C, Kakaras E. The challenge of energy storage in europe: focus on power to fuel. Journal of Energy Resources Technology, 2016, 138(4): 042002
4. Bogaerts A, Centi G. Plasma technology for CO_2 conversion: a personal perspective on prospects and gaps. Frontiers in Energy Research, 2020, 8: 111
5. Snoeckx R, Bogaerts A. Plasma technology—a novel solution for CO_2 conversion? Chemical Society Reviews, 2017, 46(19): 5805–5863
6. Qin Y, Niu G, Wang X, Luo D, Duan Y. Status of CO_2 conversion using microwave plasma. Journal of CO_2 Utilization, 2018, 28: 283–91
7. Zhu H, Huang Y, Yin S, Zhang W. Microwave plasma setups for CO_2 conversion: a mini-review. Green Energy and Resources, 2024, 2(1): 100061
8. de la Fuente J F, Kiss A A, Radoiu M T, Stefanidis G D. Microwave plasma emerging technologies for chemical processes. Journal of Chemical Technology and Biotechnology, 2017, 92(10): 2495–2505
9. Ong M Y, Nomanbhay S, Kusumo F, Show P L. Application of microwave plasma technology to convert carbon dioxide (CO_2) into high value products: a review. Journal of Cleaner Production, 2022, 336: 130447
10. Wanten B, Vertongen R, De Meyer R, Bogaerts A. Plasma-based CO_2 conversion: How to correctly analyze the performance? Journal of Energy Chemistry, 2023, 86: 180–196
11. Wiegers K, Schulz A, Walker M, Tovar G E M. Determination of the conversion and efficiency for CO_2 in an atmospheric pressure microwave plasma torch. Chemie Ingenieur Technik, 2022, 94(3): 299–308
12. Mitsingas C M, Rajasegar R, Hammack S, Do H, Lee T. High energy efficiency plasma conversion of CO_2 at atmospheric pressure using a direct-coupled microwave plasma system. IEEE Transactions on Plasma Science, 2016, 44(4): 651–656
13. van Rooij G J, van den Bekerom D C M, den Harder N, Minea T, Berden G, Bongers W A, Engeln R, Graswinckel M F, Zoethout E, van de Sanden M C M. Taming microwave plasma to beat thermodynamics in CO_2 dissociation. Faraday Discussions, 2015, 183: 233–248
14. Bongers W, Bouwmeester H, Wolf B, Peeters F, Welzel S, van den Bekerom D, den Harder N, Goede A, Graswinckel M, Groen P W, et al. Plasma-driven dissociation of CO_2 for fuel synthesis. Plasma Processes and Polymers, 2017, 14(6): 1600126
15. Chen G, Snyders R, Britun N. CO_2 conversion using catalyst-free and catalyst-assisted plasma-processes: recent progress and understanding. Journal of CO_2 Utilization, 2021, 49: 101557
16. Spencer L F, Gallimore A D. CO_2 dissociation in an atmospheric pressure plasma/catalyst system: a study of efficiency. Plasma Sources Science & Technology, 2012, 22(1): 015019
17. Salden A, Budde M, Garcia-Soto C A, Biondo O, Barauna J, Faedda M, Musig B, Fromentin C, Nguyen-Quang M, Philpott H, et al. Meta-analysis of CO_2 conversion, energy efficiency, and other performance data of plasma-catalysis reactors with the open access PIONEER database. Journal of Energy Chemistry, 2023, 86: 318–342
18. Hecimovic A, Kiefer C K, Meindl A, Antunes R, Fantz U. Fast gas quenching of microwave plasma effluent for enhanced CO_2 conversion. Journal of CO_2 Utilization, 2023, 71: 102473
19. Kiefer C K, Antunes R, Hecimovic A, Meindl A, Fantz U. CO_2 dissociation using a lab-scale microwave plasma torch: an experimental study in view of industrial application. Chemical Engineering Journal, 2024, 481: 148326
20. D'Isa F A, Carbone E A D, Hecimovic A, Fantz U. Performance analysis of a 2.45 GHz microwave plasma torch for CO_2 decomposition in gas swirl configuration. Plasma Sources Science & Technology, 2020, 29(10): 105009
21. de la Fuente J F, Moreno S H, Stankiewicz A I, Stefanidis G D. Reduction of CO_2 with hydrogen in a non-equilibrium microwave plasma reactor. International Journal of Hydrogen Energy, 2016, 41(46): 21067–21077
22. Chen G, Britun N, Godfroid T, Georgieva V, Snyders R, Delplancke-Ogletree M P. An overview of CO_2 conversion in a microwave discharge: the role of plasma-catalysis. Journal of Physics D: Applied Physics, 2017, 50(8): 084001
23. Silva T, Britun N, Godfroid T, Snyders R. Optical characterization of a microwave pulsed discharge used for dissociation of CO_2. Plasma Sources Science & Technology, 2014, 23(2): 025009
24. Belov I, Vermeiren V, Paulussen S, Bogaerts A. Carbon dioxide dissociation in a microwave plasma reactor operating in a wide pressure range and different gas inlet configurations. Journal of CO_2 Utilization, 2018, 24: 386–397
25. Leins M, Walker M, Schulz A, Schumacher U, Stroth U. Spectroscopic investigation of a microwave-generated atmospheric pressure plasma torch. Contributions to Plasma Physics, 2012, 52(7): 615–628
26. Pozar D M. Microwave Engineering. New Jersey: Wiley, 2011
27. Kiss B P, Tóth C E, Slezsák I, Kaptay G, Dobó Z. Experimental study on microwave-induced plasma-assisted premixed methane-air combustion. IEEE Transactions on Plasma Science, 2024, 52(2): 319–327
28. Yang L, Tan X, Wan X, Chen L, Jin D, Qian M, Li G. Stark broadening for diagnostics of the electron density in non-equilibrium plasma utilizing isotope hydrogen alpha lines. Journal of Applied Physics, 2014, 115(16): 163106
29. de la Fuente J F. Application of microwave plasma technology to convert CO_2 into high value products. Dissertation for the Doctoral Degree. Delft: Delft University of Technology, 2017
30. Voigt W. Uber das gesetz der intensitatsverteilung innerhalb der linien eines gasspektrums. 1912
31. Konjević N, Ivković M, Sakan N. Hydrogen Balmer lines for low electron number density plasma diagnostics. Spectrochimica Acta Part B: Atomic Spectroscopy, 2012, 76: 16–26

32. Gigosos M A, González M Á, Cardeñoso V. Computer simulated Balmer-α, -β, and -γ stark line profiles for non-equilibrium plasmas diagnostics. Spectrochimica Acta Part B: Atomic Spectroscopy, 2003, 58(8): 1489–1504
33. Leins M. Development and spectroscopic investigation of a microwave plasma source for the decomposition of waste gases. Dissertation for the Doctoral Degree. Stuttgart: Institut für Plasmaforschung der Universität Stuttgart, 2010
34. Park H, Choe W. Parametric study on excitation temperature and electron temperature in low pressure plasmas. Current Applied Physics, 2010, 10(6): 1456–1460
35. Thouin J, Benmouffok M, Freton P, Gonzalez J J. Interpretation of temperature measurements by the Boltzmann plot method on spatially integrated plasma oxygen spectral lines. European Physical Journal Applied Physics, 2023, 98: 65
36. Hibbert A, Biemont E, Godefroid M, Vaeck N. E1 transitions of astrophysical interest in neutral oxygen. Journal of Physics B: Atomic, Molecular, and Optical Physics, 1991, 24(18): 3943–3958
37. Pellerin S, Cormier J M, Richard F, Musiol K, Chapelle J. A spectroscopic diagnostic method using UV OH band spectrum. Journal of Physics D: Applied Physics, 1996, 29(3): 726–739
38. de Izarra C. UV OH spectrum used as a molecular pyrometer. Journal of Physics D: Applied Physics, 2000, 33(14): 1697–1704
39. Krähling T, Geisler S, Okruss M, Florek S, Franzke J. Spectroscopic measurements of the electron number density, electron temperature and OH(A) rotational distribution in a liquid electrode dielectric barrier discharge. Spectrochimica Acta Part B: Atomic Spectroscopy, 2015, 114: 20–26
40. Bruggeman P J, Sadeghi N, Schram D C, Linss V. Gas temperature determination from rotational lines in non-equilibrium plasmas: a review. Plasma Sources Science & Technology, 2014, 23(2): 023001
41. Dieke G H, Crosswhite H M. The ultraviolet bands of OH fundamental data. Journal of Quantitative Spectroscopy & Radiative Transfer, 1962, 2(2): 97–199
42. Chidsey I L, Crosley D R. Calculated rotational transition probabilities for the *A*−*X* system of OH. Journal of Quantitative Spectroscopy & Radiative Transfer, 1980, 23(2): 187–199
43. Atkins P, de Paula J, Keeler J. Atkins' Physical Chemistry. Oxford: Oxford University Press, 2022
44. Lozano A I, García-Abenza A, Blanco Ramos F, Hasan M, Slaughter D S, Weber T, McEachran R P, White R D, Brunger M J, Limão-Vieira P, et al. Electron and positron scattering cross sections from CO_2: a comparative study over a broad energy range (0.1–5000 eV). Journal of Physical Chemistry A, 2022, 126(36): 6032–6046
45. Itikawa Y. Cross sections for electron collisions with carbon monoxide. Journal of Physical and Chemical Reference Data, 2015, 44(1): 013105
46. Golden D E, Bandel H W, Salerno J A. Absolute total electron scattering cross sections in h_2 and d_2 for low electron energies. Physical Review, 1966, 146(1): 40–42
47. Naghma R, Vinodkumar M, Antony B. Total cross sections for O_2 and S_2 by electron impact. Radiation Physics and Chemistry, 2014, 97: 6–11
48. Dinklage A, Klinger T, Marx G, Schweikhard L. Plasma Physics. Berlin: Springer Berlin Heidelberg, 2005
49. Janzen G. Plasmatechnik. Berichte der Bunsengesellschaft für physikalische Chemie, 1992, 96(12): 1898–1898
50. Tendero C, Tixier C, Tristant P, Desmaison J, Leprince P. Atmospheric pressure plasmas: a review. Spectrochimica Acta Part B: Atomic Spectroscopy, 2006, 61(1): 2–30
51. Lieberman M A, Lichtenberg A J. Principles of Plasma Discharges and Materials Processing. Hoboken: Wiley, 2005
52. Barin I, Platzki G. Thermochemical Data of Pure Substances. 3rd ed. Weinheim: VCH Verlagsgesellschaft mbH, 1995
53. Inan U S, Gołkowski M. Principles of Plasma Physics for Engineers and Scientists. Cambridge: Cambridge University Press, 2011
54. Yubero C, García M C, Calzada M D. On the use of the Hα spectral line to determine the electron density in a microwave (2.45GHz) plasma torch at atmospheric pressure. Spectrochimica Acta Part B: Atomic Spectroscopy, 2006, 61(5): 540–544
55. Laux C O, Spence T G, Kruger C H, Zare R N. Optical diagnostics of atmospheric pressure air plasmas. Plasma Sources Science & Technology, 2003, 12(2): 125–138
56. Zhang Q, Zhang G, Wang L, Wang X, Wang S, Chen Y. Measurement of the electron density in a microwave plasma torch at atmospheric pressure. Applied Physics Letters, 2009, 95(20): 201502
57. Tao X, Bai M, Li X, Long H, Shang S, Yin Y, Dai X. CH_4–CO_2 reforming by plasma—challenges and opportunities. Progress in Energy and Combustion Science, 2011, 37(2): 113–124
58. Ricard A, St-Onge L, Malvos H, Gicquel A, Hubert J, Moisan M. Torche à plasma à excitation micro-onde: deux configurations complémentaires. Journal de Physique III, 1995, 5(8): 1269–1285
59. Calzada M D, Moisan M, Gamero A, Sola A. Experimental investigation and characterization of the departure from local thermodynamic equilibrium along a surface-wave-sustained discharge at atmospheric pressure. Journal of Applied Physics, 1996, 80(1): 46–55
60. Carbone E, D'Isa F, Hecimovic A, Fantz U. Analysis of the C_2 ($d^3\Pi_g$–$a^3\Pi_u$) Swan bands as a thermometric probe in CO_2 microwave plasmas. Plasma Sources Science & Technology, 2020, 29(5): 055003
61. Vialetto L, van de Steeg A W, Viegas P, Longo S, van Rooij G J, van de Sanden M C M, van Dijk J, Diomede P. Charged particle kinetics and gas heating in CO_2 microwave plasma contraction: comparisons of simulations and experiments. Plasma Sources Science & Technology, 2022, 31(5): 055005
62. Wolf A J, Righart T W H, Peeters F J J, Bongers W A, van de Sanden M C M. Implications of thermo-chemical instability on the contracted modes in CO_2 microwave plasmas. Plasma Sources Science & Technology, 2020, 29(2): 025005
63. Wolf A J, Righart T W H, Peeters F J J, Groen P W C, van de Sanden M C M, Bongers W A. Characterization of CO_2 microwave plasma based on the phenomenon of skin-depth-limited contraction. Plasma Sources Science & Technology, 2019, 28(11): 115022
64. Chen J, Lv Z, Zhang X, Xu T, Cheng Y. Temperature control of quartz-glass melting areas in laser additive manufacturing. Micromachines, 2024, 16(1): 29